Progress Towards a Micromachined Heat Exchanger for a Cryosurgical Probe

D. W. Hoch[1], W. Zhu[2], G. F. Nellis[1], S. D. Schuetter[1], S. A. Klein[1], and Y. B. Gianchandani[2]

[1] University of Wisconsin, Madison, Wisconsin, USA
[2] University of Michigan, Ann Arbor, Michigan, USA

ABSTRACT

Developments are described of a lithography-based micro-fabricated recuperative heat exchanger that is intended to be a component within a cryosurgical probe. A cryosurgical probe must achieve a temperature below -50°C in order to be clinically useful for the treatment of cancer. Cryosurgical probes based on the mixed gas Joule-Thomson (JT) cycle require only a recuperative heat exchanger and an expansion valve in the cold-head. Therefore, this cycle has the potential for high reliability and miniaturization. The objective of this project is to explore the potential for applying micromachining techniques to the design and fabrication of the recuperative heat exchanger. The heat exchanger must maintain high stream-to-stream thermal conductance while restricting axial conduction losses.

The 1st generation heat exchanger consists of rows of fins composed of high conductivity silicon that are bonded onto a single 100 μm thick base plate composed of low conductivity Pyrex glass. This design minimizes the number of wafers that must be bonded compared to more favorable designs based on interleaving many high conductivity silicon plates with low conductivity Pyrex spacers. However, there are several disadvantages associated with the design, most notably the fragility of the thin Pyrex base plate separating the high and low pressure streams; this limits the ability of the heat exchanger to withstand the relatively large pressure difference that is required to energize the Joule-Thomson cooling cycle. The first generation heat exchanger was fabricated and tested and the results of these tests are provided. In parallel, a bonding technique has been developed that allows multiple plates to be hermetically joined using a metallization layer. Therefore, a 2nd generation heat exchanger design is presented which overcomes many of the limitations of the 1st generation device. Specifically, it is expected to be more robust and to provide enhanced thermal performance. The design of this 2nd generation heat exchanger is discussed.

INTRODUCTION

Over the past three decades cryosurgery has become a standard treatment for several types of cancers located in easily accessible areas of the body including prostate and liver cancer. Cancerous tumors are locally destroyed using cryosurgery by exposing the malignant tissue to two repeated freeze/thaw cycles [1]. The resulting dead tissue is absorbed by the body which minimizes blood loss and the post-operative discomfort that is usually associated with excision.

Cryocoolers 14, edited by S.D. Miller and R.G. Ross, Jr.

The ultimate goal of this research effort is to develop a fully integrated micromachined cryosurgical probe based on the Joule-Thomson (JT) cooling cycle. Such a probe may have significant advantages over conventional cryosurgical probes in terms of thermal performance, size, flexibility and cost. The specific subject of this paper is the development of a microfabricated recuperative heat exchanger, the key component within the JT cycle. An overview of the 1st generation micromachined recuperative heat exchanger and experimental results are presented. The 1st generation device was designed to minimize the number of bonding steps and, as a result, is not optimally designed both in terms of mechanical reliability and thermal performance. A 2nd generation heat exchanger design has been enabled by the development of advanced bonding techniques based on a metallization process. The 2nd generation device uses a perforated plate type design and will therefore be more robust and have higher thermal performance. The design of this heat exchanger is discussed.

1ST GENERATION DESIGN AND FABRICATION

One of the challenges in the development of a micromachined J-T cooler is the recuperative heat exchanger which must simultaneously maintain good stream-to-stream heat conductance while restricting parasitic stream-wise conduction losses and supporting a large stream-to-stream pressure difference. These requirements are necessary in order to maintain a large enthalpy difference between the two fluid streams and thus achieve high cooling performance for the probe. The 1st generation heat exchanger is a planar, micromachined device in which silicon wafers are anodically bonded to either side of a very thin, low conductivity Pyrex base plate. The silicon wafers are micromachined [2] so that rows of silicon fins are left behind. These rows are aligned on the high and low pressure sides and include micro-scale fluid channels (larger on the low pressure than the high pressure) that force the fluid into intimate contact with the fins.

This design is in contrast to conventional recuperative heat exchangers for cryosurgery that use either perforated plate designs in which high conductivity copper plates are interleaved with stainless steel spacers [3] or finned tube designs that use one or more finned tubes wound on a mandrel. Silicon has thermal conductivity that is similar to copper, and Pyrex has thermal conductivity that is an order of magnitude less than stainless steel; this combination of very high and low thermal conductivity suggests that a silicon and Pyrex composite heat exchanger will be attractive. In order to allow adequate thermal communication between the streams, preliminary simulation of an optimized design [4] suggest that when using a mixture of hydrocarbons at a working pressure of 20 bar, the Pyrex base plate between the high pressure channel and low pressure channel can be no thicker than about 100 μm in order to provide adequate refrigeration power. Figure 1 shows a fabricated micro recuperative heat exchanger. The size of this device is 6 cm × 1.5 cm with 2.5 mm total thickness.

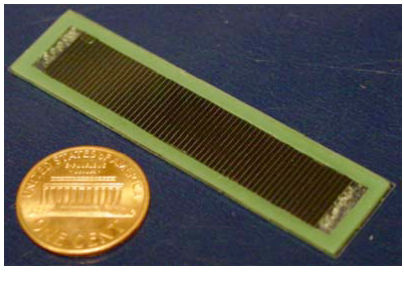

Figure 1. 1st generation heat exchanger illustrating the Pyrex cap, silicon fins and green anodic glass-frit bond.

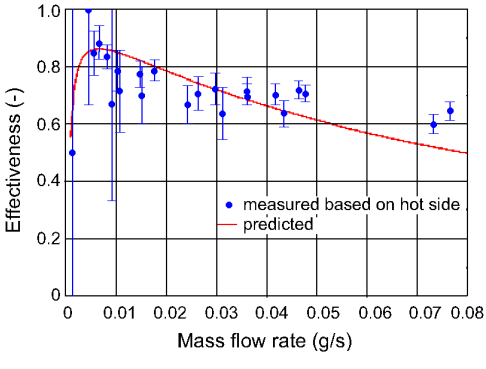

Figure 2. Measured effectiveness based on hot side energy balance and the predicted effectiveness using the micro heat exchanger model as a function of the mass flow rate.

MEASURED RESULTS

The glass frit bonding process used to join the Pyrex outer caps to the Pyrex base plate in the 1st generation design does not provide a hermetic seal and this has prevented its installation into a thermal vacuum facility. Instead, the heat exchanger was placed into a cavity within a piece of Styrofoam and surrounded by fiberglass insulation in an effort to minimize the parasitic heat load. N-butane was used as the working fluid in an open loop Joule-Thomson cycle and expanded through an orifice. The self-cooling data are limited to relatively small temperature differences due to the reduced JT effect associated with the small pressure difference that could be supported across the base plate. The pressure difference anticipated for a cryosurgical probe may be as high as 1400 kPa (200 psi) whereas the testing was limited to less than 70 kPa (10 psi) in order to avoid fracturing the base plate. A thicker base plate would provide greater structural integrity, but the increased thermal resistance between fluid streams would further reduce cooling power.

The predicted and measured effectiveness as a function of mass flow rate (based on the hot side energy balance) are illustrated in Figure 2. The effectiveness of the heat exchanger (ε) is defined as the ratio of the heat transfer rate within the heat exchanger to the maximum possible heat transfer rate for the given input fluid conditions. The effectiveness can be computed based on an energy balance for either the hot or cold side of the heat exchanger: ε_h or ε_c, respectively:

$$\varepsilon_h = \frac{\dot{q}_{HX,h}}{\dot{q}_{HX,max}} \qquad \textbf{or} \qquad \varepsilon_c = \frac{\dot{q}_{HX,c}}{\dot{q}_{HX,max}} \tag{1}$$

where $\dot{q}_{HX}$ is the actual heat transfer (evaluated from an energy balance on the hot or cold side) and $\dot{q}_{HXmax}$ is the ideal heat transfer in perfect conditions. The error bars in Fig. 2 show propagated uncertainty in the effectiveness based on uncertainty in the thermocouple temperature measurements. Note that the uncertainty increases as the mass flow rate is reduced due to the smaller temperature differences that are required to compute the effectiveness. The measured results agree with the theoretical model for the flow rates that are consistent with accurate measurements. The results of the 1st generation tests indicate the limitations of the design, but also validate the ability of the computer model to predict the thermal performance of the heat exchanger.

Therefore, these modeling techniques have been used to develop a more robust design enabled by the development of more advanced, multi-wafer joining techniques that will provide cooling performance comparable to commercially available cryosurgical probes.

SECOND GENERATION HEAT EXCHANGER MODEL

A new bonding technique that shows the potential to hermetically join many multiple plates has been developed in parallel with the 1st generation heat exchanger testing. The joining technique uses a metallization layer that is applied to the wafers and accommodates the bond.

This 2nd generation heat exchanger design is similar to most perforated plate heat exchangers: high conductivity silicon plates are alternated with low conductivity Pyrex spacers. Figure 3 illustrates the 2nd generation design showing the perforated plate heat exchanger concept. Many, narrow slots are machined into the silicon plate in order to provide the two streams with a large amount of surface area for heat exchange. The plates are divided into two regions by the Pyrex spacer (indicated by the gray area in Fig. 3). The high pressure region allows flow of the high pressure working fluid in one direction (into the paper in Figure 3) while the low pressure region allows flow of the low pressure working fluid in the opposite direction. The high and low pressure regions are separated and sealed from each other via bonds formed between the plate and the spacer. The heat transferred from the high pressure fluid into the silicon plate material is conducted through the silicon plate into the low pressure region where it is transferred finally to the low pressure fluid. Many of these plate/spacer sets are stacked up to achieve high effectiveness.

A numerical model has been developed to optimize the geometry of the heat exchanger; the basic structure of the model is the thermal-fluid simulation of a single plate operating at the average

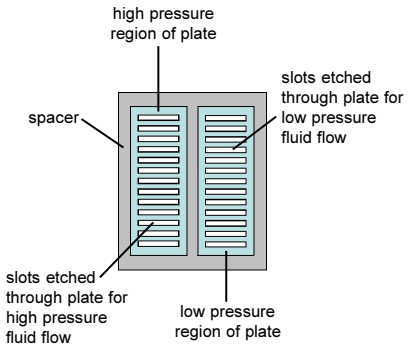

Figure 3. Concept for micromachined perforated plate heat exchanger.

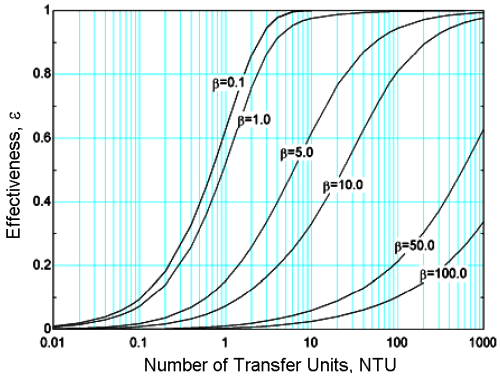

Figure 4. Fin effectiveness as a function of fin number of transfer units for several values of the fin constant.

condition within the heat exchanger. The Reynolds numbers for the flow through the slots on the high and low pressure sides (Re_h and Re_c) are given by:

$$Re_h = \frac{\rho_h d_{h,h} u_{m,h}}{\mu_h} \tag{2}$$

$$Re_c = \frac{\rho_c d_{h,c} u_{m,c}}{\mu_c} \tag{3}$$

where ρ is the fluid density, u_m is the mean velocity, and μ is the fluid viscosity; the subscripts h and c refer to the high and low pressure fluids, respectively. The variables d_h is the hydraulic diameter of the passage.

For laminar flow (Re < 2300), the Nusselt numbers under fully developed conditions for a rectangular duct subject to a constant wall temperature (Nu_{lam}) are given by Rohsenow et al. [5]:

$$Nu_{lam,h} = 7.541\left(1 - 2.61\alpha_h + 4.97\alpha_h^2 - 5.119\alpha_h^3 + 2.702\alpha_h^3 + 0.548\alpha_h^4\right) \tag{4}$$

$$Nu_{lam,c} = 7.541\left(1 - 2.61\alpha_c + 4.97\alpha_c^2 - 5.119\alpha_c^3 + 2.702\alpha_c^3 + 0.548\alpha_c^4\right) \tag{5}$$

where α_h and α_c are the aspect ratios of the slot:

$$\alpha_h = \frac{\min\left(w_{s,h}, L_f\right)}{\max\left(w_{s,h}, L_f\right)} \tag{6}$$

$$\alpha_c = \frac{\min\left(w_{s,c}, L_f\right)}{\max\left(w_{s,c}, L_f\right)} \tag{7}$$

and w_s and L_f are the width and length of the slot, respectively. The Nusselt number under fully developed conditions for a turbulent flow (Nu_{turb} and Nu_{turb}) is predicted by the Gnielinski [6]:

$$Nu_{turb,h} = \frac{\left(f_{turb,h}/8\right)\left(Re_h - 1000\right)Pr_h}{1 + 12.7\sqrt{f_{turb,h}/8}\left(Pr_h^{2/3} - 1\right)} \tag{8}$$

$$Nu_{turb,c} = \frac{\left(f_{turb,c}/8\right)\left(Re_c - 1000\right)Pr_c}{1 + 12.7\sqrt{f_{turb,c}/8}\left(Pr_c^{2/3} - 1\right)} \tag{9}$$

where f_{turb} is the friction factor for fully developed turbulent flow, and Pr is the Prandtl number, computed according to:

$$Pr_h = \frac{c_{p,h}\,\mu_h}{k_h} \tag{10}$$

$$Pr_c = \frac{c_{p,c}\,\mu_c}{k_c} \tag{11}$$

where c_p is the constant pressure specific heat capacity and k is the thermal conductivity of the fluid.

The friction factor for fully developed, turbulent flow can be calculated according to Petukhov et al. [7]:

$$f_{turb,h} = \left(0.79\ln\left(Re_h\right) - 1.64\right)^{-2} \tag{12}$$

$$f_{turb,c} = \left(0.79\ln\left(Re_c\right) - 1.64\right)^{-2} \tag{13}$$

These correlations are selected because they are valid down to a Reynolds number of 3000; lower Reynolds numbers are assumed to correspond to laminar flow (which is conservative relative to the predicted Nusselt number). These Nusselt number correlations are conservative both because the enhancement in the heat transfer related to the developing region of the channel is not accounted for and also because the two-phase heat transfer that occurs over the majority of the heat exchanger for fluid mixture working fluids will be characterized by larger heat transfer coefficients [8]. The heat transfer coefficients (*htc*) are:

$$htc_h = \frac{Nu_h\,k_h}{d_h} \tag{14}$$

$$htc_h = \frac{Nu_h\,k_h}{d_h} \tag{15}$$

It is assumed that the fluid will completely mix in the space between adjacent plates so that the temperature of the hot fluid is uniform as it enters all of the slots on the high pressure side ($T_{h,in}$) and the temperature of the cold fluid is uniform as it enters all of the slots on the low pressure side ($T_{c,in}$). The fluid passing through each fin row does not maintain a constant temperature; rather, its temperature will change due to its finite capacity rate. As a result of this, as well as axial (i.e., in the flow direction) temperature variations in the fin material, it is incorrect and non-conservative to use conventional fin equations that assume constant fluid temperature. A numerical model that solves the coupled differential equations governing the two-dimensional temperature distribution in the fluid and the fin material has been developed, validated, and non-dimensionalized. The result of the numerical model is the prediction of the fin effectiveness (ε_f) as a function of the fin constant (β_f) and the fin number of transfer units (NTU_f), shown in Figure 4.

The fin effectiveness (ε_f) is defined as the ratio of the actual heat transfer through the base of the fin ($\dot{q}_f$) to the maximum possible heat transfer; i.e., the heat transfer that would occur if the fluid temperature was reduced to the base temperature of the fin (T_b). On the high-pressure side this leads to:

$$\varepsilon_{f,h} = \frac{\dot{q}_f}{\dot{m}\,c_{p,h}\left(T_{h,in} - T_{b,h}\right)} \tag{16}$$

where $T_{b,h}$ is the base temperature of the fins (the material between adjacent slots) on the high-pressure side of the heat exchanger. On the low-pressure side, the fin effectiveness is:

$$\varepsilon_{f,c} = \frac{\dot{q}_f}{\dot{m}\,c_{p,c}\left(T_{b,c} - T_{c,in}\right)} \tag{17}$$

The fin constants (β_f) and fin number of transfer units (NTU_f) are defined as:

$$\beta_{f,h} = \frac{L_f}{2}\sqrt{\frac{2htc_h}{k_p\, w_{f,h}}} \tag{18}$$

$$\beta_{f,c} = \frac{L_f}{2}\sqrt{\frac{2htc_c}{k_p\, w_{f,c}}} \tag{19}$$

$$NTU_{f,h} = \frac{2L_f\, t_p\, htc_h\, N_{f,h}}{\dot{m}\, c_{p,h}} \tag{20}$$

$$NTU_{f,c} = \frac{2L_f\, t_p\, htc_c\, N_{f,c}}{\dot{m}\, c_{p,c}} \tag{21}$$

where k_p is the plate thermal conductivity, t_p is the plate thickness, N_f is the number of fins, w_f is the width of the material between slots, and $\dot{m}$ is the mass flow rate. Each of the curves for ε_f as a function of NTU_f in Fig. 4 can be approximately represented by Eqs. (22) and (23):

$$\varepsilon_{f,h} = 1 - \exp\left[-a\left(\beta_{f,h}\right) NTU_{f,h}^{\,b(\beta_{f,h})+c(\beta_{f,h})\ln(NTU_{f,h})} \right] \tag{22}$$

$$\varepsilon_{f,c} = 1 - \exp\left[-a\left(\beta_{f,c}\right) NTU_{f,c}^{\,b(\beta_{f,c})+c(\beta_{f,c})\ln(NTU_{f,c})} \right] \tag{23}$$

Equations for *a, b*, and *c* as functions of the fin constant are listed below and the required constants are contained in Table 1; these constants are obtained through best fits to the numerical results.

$$a(\beta_f) = \exp\left[-a_o\, \beta_f^{(a_1+a_2\beta_f+a_3\beta_f^2)} \right] \tag{24}$$

$$b(\beta_f) = \sum_{i=0}^{5} b_i \left[\log_{10}(\beta_f)\right]^i \tag{25}$$

$$c(\beta_f) = \sum_{i=0}^{6} c_i \left[\log_{10}(\beta_f)\right]^i \tag{26}$$

Equations (22) through (26) allow the effectiveness of the fins on both sides of the plate to be calculated from the fin constant and number of transfer units. The maximum error associated with the use of these curve fits in the range $0.01 < NTU < 1000$ and $0.01 < \beta < 5$ is 3.2% and the rms error over this range is 0.04%.

Equations (16) and (17) may be re-written in the form of thermal resistance (R_f) between the fluid inlet temperature and the temperature at the base of the fins:

$$\dot{q}_f = \frac{\left(T_{h,in} - T_{b,h}\right)}{R_{f,h}} \quad \text{where } R_{f,h} = \frac{1}{\varepsilon_{f,h}\, \dot{m} c_{p,h}} \tag{27}$$

$$\dot{q}_f = \frac{\left(T_b - T_{c,in}\right)}{R_{f,c}} \quad \text{where } R_{f,c} = \frac{1}{\varepsilon_{f,c}\, \dot{m} c_{p,c}} \tag{28}$$

The thermal resistance from the center-line of the material that separates the high and low pressure streams to the fluid inlet temperature (R_{plate}) is larger than the thermal resistance, R_f due to the additional conduction resistance represented by the plate material:

$$R_{plate.h} = R_{f,h} + \frac{\left(w_p + \frac{w_{sp}}{2}\right)}{N_{f,h}\, k_p\, t_p \left(w_{s,h} + w_{f,h}\right)} \tag{29}$$

Table 1. Constants required for fin effectiveness solution.

Index, i	a_i	b_i	c_i
0	0.297925119	0.927242296	-0.049798866
1	1.492222514	-0.071330646	-0.106555996
2	-0.081006078	0.061074063	0.020416859
3	0.002369923	0.026320276	0.141444269
4	-	-0.067908807	0.032192166
5	-	-0.03036481	-0.048599571
6	-	-	-0.018543303

$$R_{plate,c} = R_{f,c} + \frac{\left(w_p + \frac{w_{sp}}{2}\right)}{N_{f,c} k_p t_p \left(w_{s,c} + w_{f,c}\right)} \tag{30}$$

The total rate of heat transfer for each plate is therefore:

$$\dot{q}_f = \frac{\left(T_{h,in} - T_{cl}\right)}{R_{plate,h}} \tag{31}$$

$$\dot{q}_f = \frac{\left(T_{cl} - T_{c,in}\right)}{R_{plate,c}} \tag{32}$$

where T_{cl} is the temperature at the center-line of the plate. Combining Eqs. (31) and (32) leads to:

$$\dot{q}_f = \frac{\left(T_{h,in} - T_{c,in}\right)}{R_{plate,h} + R_{plate,c}} \tag{33}$$

and the effectiveness of an individual plate (ε_p) is therefore given by the ratio of the actual heat transfer to the maximum possible heat transfer for the plate:

$$\varepsilon_p = \frac{\dot{q}_f}{MIN\left(\dot{m}c_{p,h}, \dot{m}c_{p,c}\right)\left(T_{h,in} - T_{c,in}\right)} = \frac{1}{MIN\left(\dot{m}c_{p,h}, \dot{m}c_{p,c}\right)\left(R_{plate,h} + R_{plate,c}\right)} \tag{34}$$

The axial resistance of a single spacer is (R_{spacer}) is:

$$R_{spacer} = \frac{t_{sp}}{k_{spacer} A_{spacer}} \tag{35}$$

and so the total effectiveness of the heat exchanger, including a penalty for axial conduction, (ε) can be estimated according to:

$$\varepsilon = 1 - \left[1 + \frac{N_p \varepsilon_p}{1 - \varepsilon_p}\right]^{-1} - \frac{1}{N_p R_{spacer} MIN\left(\dot{m}c_{p,h}, \dot{m}c_{p,c}\right)} \tag{36}$$

The equivalent number of transfer units (NTU_{eq}) associated with a continuous heat exchanger with no axial conduction is:

$$NTU_{eq} = \begin{cases} \dfrac{1}{C_r - 1} \ln\left(\dfrac{\varepsilon - 1}{\varepsilon C_r - 1}\right) & \text{if } C_r < 1 \\ \dfrac{\varepsilon}{1 - \varepsilon} & \text{if } C_r = 1 \end{cases} \tag{37}$$

where C_r is the capacity ratio:

$$C_r = \frac{MIN\left(\dot{m}c_{p,h}, \dot{m}c_{p,c}\right)}{MAX\left(\dot{m}c_{p,h}, \dot{m}c_{p,c}\right)} \tag{38}$$

The equivalent conductance associated with the heat exchanger performance (UA_{eq}) is therefore:

$$UA_{eq} = MIN\left(\dot{m}c_{p,h}, \dot{m}c_{p,c}\right) NTU_{eq} \tag{39}$$

The design of the heat exchanger requires both the equivalent conductance and the pressure loss. It is non-conservative to neglect the effect of the developing region when evaluating the pressure loss. The apparent friction factor for developing, laminar flow ($f_{app,lam}$) depends on the Reynolds number, the aspect ratio of the slot, and the dimensionless thickness of the plate. For an aspect ratio of zero (i.e., parallel plates), the apparent friction factor is given by Rohsenow et al. [5]. The apparent friction factor for turbulent flow may be higher, although the developing region is less important when the flow is turbulent. The apparent laminar or fully developed turbulent friction factor is selected based on the Reynolds number; a Reynolds number of 3000 is used to indicate transition. The viscous pressure loss (Δp_v) is captured by the friction factor:

$$\Delta p_{v,h} = \frac{1}{2}\rho_h u_{m,h}^2 f_{app,h} \frac{t_p}{d_{h,h}} \tag{40}$$

$$\Delta p_{v,c} = \frac{1}{2}\rho_c u_{m,c}^2 f_{app,c} \frac{t_p}{d_{h,c}} \tag{41}$$

In addition to the viscous pressure loss, there are contraction and expansion effects that must be considered. The flow contraction and expansion pressure loss coefficients (K_c and K_e) for both sides are, conservatively, assumed to be unity. The inertial pressure losses (Δp_i) are therefore:

$$\Delta p_{i,h} = \frac{1}{2}\rho_h u_{m,h}^2 \left(K_e + K_i\right) \tag{42}$$

$$\Delta p_{i,c} = \frac{1}{2}\rho_c u_{m,c}^2 \left(K_e + K_i\right) \tag{43}$$

The total pressure loss (Δp) is the sum of the inertial and viscous pressure losses over all of the plates.

$$\Delta p_h = N_p \left(\Delta p_{i,h} + \Delta p_{v,h}\right) \tag{44}$$

$$\Delta p_c = N_p \left(\Delta p_{i,c} + \Delta p_{v,c}\right) \tag{45}$$

2ND GENERATION HEAT EXCHANGER OPTIMIZATION

A manufacturing constraint associated with the micromachining process that controls the design is related to the length of the slots in the silicon plate. As the slot length increases, the ability to control the slot width is lost; eventually, the over-etching during the KOH process may become severe enough that all of the fin material is removed. Therefore, the slot length must be less than 10 times the slot width, and webs that span the width of the slot are added to create a series of smaller, more robust openings within the original slot. Additionally, the thickness of each web should be twice the width of the slot. These constraints are integrated with the numerical model described above; the model is implemented in the mathematical software EES - Engineering Equation Solver [9].

The length and width of each plate and spacer was set to 20 mm to maximize the yield of each silicon-Pyrex mask while still providing performance comparable to commercially available

cryosurgical probes. A Joule-Thomson cycle model was developed that takes the predicted, equivalent heat exchanger conductance, UA_{eq} and pressure drop on each side, Δp_h and Δp_c, as inputs and calculates a corresponding cooling capacity and probe tip temperature for a given mass flow rate. The concentration of the working fluid is optimized as discussed in [10]. Figure 5 illustrates a maximum cooling power at a flow rate of 0.55 g/s. Figure 6 shows the predicted cooling power associated with several web configurations as a function of the probe tip temperature for a 20mm x 20mm heat exchanger with 50 silicon plates at the optimal mass flow rate of 0.55 g/s. Figure 6 indicates a plate with 12 webs per slot provides the best performance above 132 K. The performance of a commercially available cryosurgical probe is also included in Figure 6. The pressure drop as a function of the mass flow rate through the cold side of the heat exchanger is illustrated in Figure 7 for several web configurations. The pressure drop through the hot side of the heat exchanger is approximately an order of magnitude smaller than the cold side due to the relatively large difference in densities of the two streams. The operating conditions used during the optimization and the corresponding geometry are listed in Table 2.

SUMMARY

This paper describes developments towards a microfabricated recuperative heat exchanger that is intended to be a component within a cryosurgical probe based on the mixed gas Joule-Thomson (JT) cycle. A first generation heat exchanger has been designed and tested that utilizes anodic bonding to join rows of fins composed of high conductivity silicon onto a single 100µm base plate composed of low conductivity Pyrex glass. This design minimizes the number of wafers that must be bonded, but the thin Pyrex plate required to minimize axial conduction along the length of the heat exchanger limits the ability of the heat exchanger to withstand the relatively large pressure difference that is required by a Joule-Thomson cooling cycle. However, numerous manufacturing constraints have been overcome during the development of this design and the data collected have allowed the heat exchanger model to be verified over a limited temperature range.

In parallel, a bonding technique has been developed that shows the potential to allow multiple plates to be hermetically joined using a metallization layer. This new joining technique and the verified numerical model have been used to design a 2nd generation heat exchanger that uses high conductivity silicon plates that are alternated with low conductivity Pyrex spacers. The 2nd generation heat exchanger has been optimized so that it is robust to the stream-to-stream pressure difference and provides enhanced thermal performance as compared to the 1st generation design. Our intention is to build several proof-of-concept 2nd generation heat

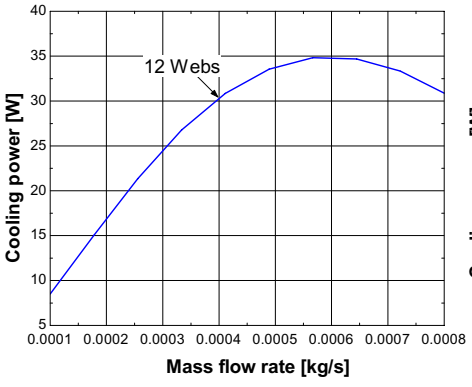

Figure 5. Cooling power as a function of the mass flow rate for the 12 web configuration.

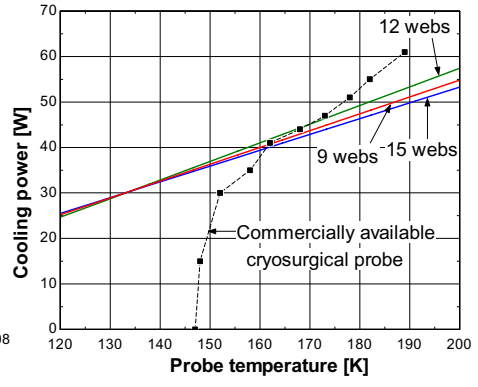

Figure 6. Cooling power as a function of the probe tip temperature for several web configurations. The cooling power of a commercially available probe is also included.

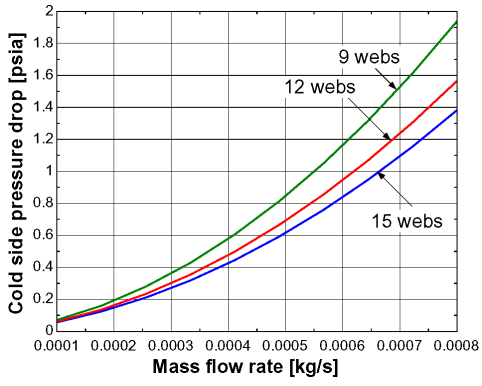

Figure 7. Pressure drop through cold side of heat exchanger as a function of mass flow rate for several web configurations.

Table 2. Parameters used during optimization of heat exchanger.

Parameters	
Heat exchanger length	20mm
Heat exchanger width	20mm
Mass flow rate	0.55 g/s
Hot side inlet pressure	1500 kPa
No. of fin rows, N_f	170
No. of slots in a row, N_s	13
No. of web, N_{web}	12
Length of each slot, L_s	500 µm
Length of each fin, L_f	7700 µm
Length of each web, L_{web}	100 µm
Width of each slot, w_s	50 µm
Distance between each slot row, w_f	50 µm
Thickness of Si plate, t_p	500 µm
Thickness of glass spacer, t_{sp}	250 µm
Minimum distance from edge of slot to Pyrex spacer, W_p	100 µm

exchangers based on the optimized design that can be installed into a thermal vacuum chamber and performance tested. The experimental results will allow further verification and improvement of the computer model.

ACKNOWLEDGEMENT

This work was funded by a grant from the US National Institutes of Health (R21 EB003349-02).

REFERENCES

1. Dobak, J., "A Review of Cryobiology and Cryosurgery," *Advances in Cryogenic Engineering*, Vol. 43 (1998), pp. 889-896.
2. Zhu, W., Hoch, D.W., Nellis, G.F., Klein, S.A., and Gianchandani, Y.B., "A Planar Glass/Si Micromachining Process for the Heat Exchanger in a J-T Cryosurgical Probe," presented at the 2006 Solid-State Sensors, Actuator, and Microsystem Workshop, Hilton Head Island, SC (2006).
3. Dobak, J., Marguardt, E.D., and Radebaugh, R., "A Cryogenic Catheter for Treating Heart Arrhythmia," *Advances in Cryogenic Engineering*, Vol. 43 (1998), pp. 903-910.
4. Frank, M., *Recuperative Heat Exchanger for a MEMS Cryoprobe*, M.S. Thesis, University of Wisconsin, Dept. of Mechanical Engineering, 2004.
5. Rohsenow, W.M., Hartnett, J.P., and Cho, Y.I, *Handbook of Heat Transfer*, McGraw-Hill, New York (1998).
6. Gnielinski, V., *Int. Chem. Eng.*, Vol. 16 (1976), p. 359.
7. Pethukhov, B.S., in Irvine, T.F., and Hartnett, J.P., eds., *Advances in Heat Transfer*, Vol. 6, Academic Press, NY (1970).
8. Nellis, G.F., Hughes, C.B., and Pfotenhauer, J.M., "Heat Transfer Coefficient Measurements for Mixed Gas Working Fluids at Cryogenic Temperatures," *Cryogenics*, Vol. 45, No. 8 (August 2005), pp. 546-556.
9. Klein, S. A., 2006, *EES-Engineering Equation Software*, F-Chart Software, http://www.fchart.com.
10. F. Keppler, G. Nellis, and S. Klein, "Optimization of the Composition of a Gas Mixture in a Joule-Thomson Cycle," *International Journal of Heating, Ventilation, Air Conditioning, and Refrigeration Research,* Vol. 10, No. 2 (2004), pp. 213-230.